# Optimizing the beam selection for non-coplanar VMAT by using simulated annealing approach

Franklin Okoli, Julien Bert, Salih Abdelaziz, Nicolas Boussion, Dimitris Visvikis

# Optimizing the beam selection for non-coplanar VMAT by using simulated annealing approach

Franklin Okoli, Julien Bert, Salih Abdelaziz, Nicolas Boussion, Dimitris Visvikis

*Abstract*—Non-coplanar VMAT treatment can achieve better organ-at-risk (OAR) avoidance by orienting the radiation beams in a different geometric plane relative to the patient. However, determining the optimal set of beam orientations is challenging due to the additional degrees of freedom. The objective of this study was to use Simulated Annealing (SA) for beam selection in non-coplanar VMAT optimization context. SA method was combined with a direct leaf trajectory optimization approach to obtain a set of globally optimal beams which serve as control points for the treatment trajectory. Proposed method was evaluated through the TG119 benchmark and two clinical cases (prostate and liver cancers). Finally, the SA beam selection method was compared to the standard coplanar and non-coplanar beam selection approach. The results showed an accurate delivery of the prescription dose to the target tumor volume in all cases. Generally, not on every organ, the non-coplanar SA method showed better organ-at-risk (OAR) sparing compared to the coplanar and non-coplanar greedy method. This work demonstrates that optimized non-coplanar beam orientations using the proposed SA method can be more clinically interesting than coplanar method in some specific patient cases.

*Index Terms*—Radiotherapy; treatment planning optimization; non-coplanar VMAT; beam selection; simulated annealing

## I. Introduction

Volumetric modulated arc therapy (VMAT) is a radiotherapy treatment delivery technique that involves the rotational delivery of radiation [1]. The main goal in VMAT is to deliver rapidly the conformal dose to the tumor, minimizing the dose to the surrounding organs at risk. In non-coplanar VMAT, the gantry carries the radiation beam and the patient couch rotate simultaneously to change the radiation beam orientation. At the same time, the radiation fluence intensity and the aperture shape change at each control point to obtain a prescribed dose distribution within the tumor in the patient. It has been argued that non-coplanar VMAT could lead to superior treatment plans and should be used in treatment planning [2]. A major advantage is that non-coplanar VMAT can achieve better organ-at-risk (OAR) avoidance by orienting the radiation beams in a different geometric plane relative to the patient. Results from studies targeting different cancer locations, (intracranial, sinonasal, liver, etc.), have confirmed these [3], [4], [5].

In non-coplanar VMAT, determining the optimal set of beam orientations for a clinical case is challenging due to the additional degrees of freedom [6]. Not all beam combinations can necessarily be evaluated because for each of them a complete

Franklin Okoli, Julien Bert, Nicolas Boussion and Dimitris Visvikis are with the LaTIM, INSERM UMR1101, Brest France (E-mail: franklin.okoli@univ-brest.fr, julien.bert@univ-brest.fr, nicolas.boussion@chu-brest.fr, dimitris.visvikis@univ-brest.fr).
Salih Abdelaziz is with LIRMM, CNRS, Montpelier France (E-mail: Salih.Abdelaziz@lirmm.fr).

Direct Aperture Optimization [7] (DAO) has to be performed in order to define the multi-leaf collimator layout. Such a brute force operation remains too demanding in terms of memory storage and time computation to be used in a clinical context. Several approaches have been proposed to efficiently explore an optimal set of beams within this large space of solutions. For example, methods using genetic algorithm, greedy strategy, look ahead strategy and gradient strategy have been used for non-coplanar VMAT beam selection [8], [9]. The main drawback of using beam angle selection methods is that it presents highly non-convex combinatorial optimization problems with many local minima. Therefore, considering the large number of possible solutions, most beam angle selection methods evaluate the fluence contribution of the beams on a limited portion of the solution space. A recent approach from [10] proposes to estimate individual scoring on every beam in order to eliminate suboptimal beams and perform the planning using a reduced set of beams.

However, in order to obtain a high quality non-coplanar VMAT treatment plan the entire space of candidate beams during the selection have to be explored [11]. Within this context, we propose to investigate the dosimetric performance of a simulated annealing (SA) inspired algorithm for beam selection in non-coplanar VMAT treatment planning.

## II. Materials and Methods

### A. Non-coplanar VMAT planning methodology

Given the 3D computed tomography (CT) image of a cancer patient, the entire volume contains a set of $\mathbb{V}$ discrete voxels. The incident radiation beam $b$ for patient treatment at each orientation can be decomposed into a set of beamlets.

The dose received by a voxel $j \in \mathbb{V}$ is denoted as $d_j$ and the intensity of an incident beamlet $i \in b$ with fluence intensity $x_i$. $\mathbb{B}$ denotes the set of candidate beam angles that are available for the VMAT treatment planning. Such that $b \in \mathbb{B}$ a set of equally spaced couch-gantry angle pairs that constitute a $4\pi$ space. At the initial stage, the infeasible or collision-prone configurations are removed from $\mathbb{B}$. The dose influence matrix, $\boldsymbol{D}$, expresses the relationship between the dose received by a voxel $d_j$ and a beamlet of unit fluence intensity $x_i$, such that:

$$d_j = \sum_{i \in b} D_{ji} x_i \qquad (1)$$

Given a dose prescribed by the physician $\hat{\boldsymbol{d}}$ to be delivered to the tumor, our objective function minimizes the least-square deviation between the prescribed dose and the actual dose received by the tumor voxels.

$$f(\boldsymbol{d}) = \frac{1}{N_t} \sum_{j \in \mathbb{V}_\approx} p^+ (d_j - \hat{d}_j)^2 + \frac{1}{N_o} \sum_{j \in \mathbb{V}_\rtimes} p^- (d_j - \hat{d}_j)^2 \quad (2)$$

where $\mathbb{V}_\approx \subset \mathbb{V}$ denotes the tumor voxels with cardinality $|\mathbb{V}_\approx| = N_t$ and $\mathbb{V}_\rtimes \subset \mathbb{V}$ denotes the organ-at-risk voxels with cardinality $|\mathbb{V}_\rtimes| = N_o$. $p^+$ is a penalty factor for controlling the relative importance of the target tumor voxels and $p^-$ is the penalty factor for controlling the relative importance of organ-at-risk voxels. At an initial stage, the dose influence matrix $\boldsymbol{D}^{(nv \times nb)}$ is calculated for each beam angle $b \in \mathbb{B}$ in the set of all candidate beam angles. Where nv is the number of voxels in the patient CT image and nb is the number of beamlets used for treatment.

In this work, only the beam selection was investigated. The general non-coplanar VMAT planning method proposed in [9] was used. In [9], the greedy approach is used to select the beams that gives the greatest improvement to the objective function at each iteration in the first step. The second step is to create a trajectory by solving a traveling salesman problem to connect all the optimal control points obtained from beam selection. Finally a direct leaf optimization (DLO) [12] is performed to obtain the final plan using the new trajectory. The direct leaf method optimizes directly the multileaf collimator (MLC) trajectory for radiation delivery in a sliding window fashion while taking into account MLC and machine constraints. This method has the advantage of avoiding the arc-sequencing step used in DAO so that plan quality is not compromised. The problem formulation is approximately convex, and its solution can be found using commercially available solvers. In order to obtain the best possible treatment plan, the entire beam angle space needs to be explored for a global solution. Therefore, simulated annealing method for the beam angle selection was proposed in this work in the place of the greedy approach. SA method enables the exploration of the entire space of the candidate beam angles in an efficient manner.

### B. Simulated annealing for beam selection

Simulated annealing (SA) is a state-of-the-art heuristic method with the ability to produce an approximately global solution to a combinatorial optimization problem. It is a technique inspired from the annealing process in metallurgy with the notion of slow cooling interpreted as a slow decrease in the probability of accepting sub-optimal solutions as the algorithm proceeds, as follows:

$$P(\Delta f) \approx \exp(-\Delta f / T_\rho) \quad (3)$$

Where $\rho$ is the iteration number, $\Delta f$ is the cost function value difference between $\rho$ and $\rho - 1$ iterations. The annealing temperature at the $\rho th$ iteration $T_\rho$ is decreased with cooling rate $\lambda$ as given by the exponential annealing schedule described by:

$$T_\rho = T_{\rho-1} \times (1 - \lambda) \quad (4)$$

The cooling factor $\lambda$ is a user-defined value in the range $[0, 1]$. The choice of the exponential annealing schedule is

motivated by the need to have a faster algorithm execution due to the large number of beam angles being evaluated. A logarithmic annealing schedule can be used as they have been shown to be sufficient to obtain a global minimum [13]. But such a logarithmic annealing schedule would lead to a longer execution time. Simulated annealing has already been successfully applied in different contexts such as intensity-modulated radiotherapy (IMRT) planning [14] and prostate brachytherapy planning [15]. We propose to combine the SA method with direct leaf trajectory optimization in order to include machine parameter constraints during the non-coplanar VMAT beam selection phase.

The proposed algorithm starts initially with a set of non-coplanar candidate beams $\mathbb{B}$ and an initial temperature $T_{init}$. The output is a set containing the optimal beam combination $\mathbb{K}^*$. At each iteration, a beam $b^*$ in the non-coplanar VMAT treatment plan is selected at random to be replaced by a candidate beam not included in the treatment plan. The objective function value (f) of this beam angle combination is calculated by solving the direct leaf trajectory optimization. In this approach, when comparing different beam angle combinations, both machine and MLC constraints are taken into account. The resulting beam combination is accepted as the best one if the acceptance probability $P_\rho$ is greater than a threshold chosen by the user. The cooling temperature is progressively decreased by a factor $\lambda$ to control the probability of accepting a new solution. The algorithm is stopped when the cooling temperature $T_\rho$ is less than a chosen threshold for the final temperature $T_{final}$.

The choice of the initial and final temperatures $T_{init}, T_{final}$ influences the cooling rate and hence the speed of convergence [16]. If $T_{init}$ is set too high, a lot of time is spent at the beginning of the algorithm and if set too low, the algorithm terminates with a local solution in a very short time. $T_{init}$ is chosen automatically using an analytical relationship that maximizes the probability of accepting state transitions during the initial search in the solution space [17]. Specifically:

$$T_{init} = \frac{-\Delta f_{max}}{\ln(P(-\Delta f_{max}))} \quad (5)$$

where $\Delta f_{max} = \max(f(\mathbb{K}_\rho) - f(\mathbb{K}_j))$ defines the maximum deterioration in the objective function value from solution $\mathbb{K}_\rho$ to a neighboring solution $\mathbb{K}_j$. In the same way, a $T_{final}$ set too high delays the algorithm termination and if set too low, the algorithm terminates with a local solution. Identically to $T_{init}$, $T_{final}$ is calculated in the same way but considering the minimum deterioration in the objective function $\Delta f_{min}$.

### C. Direct leaf trajectory optimization details

The direct leaf trajectory optimization was proposed to generate a deliverable VMAT plan in a single step by directly optimizing the trajectory of the multileaf collimator [12]. It is written as:

$$\underset{\mathbf{x}}{\text{minimize}} \ f(\mathbf{d}) \tag{6a}$$

$$\text{subject to: } d_j = \sum_{k=1}^{k=K} \sum_{n=1}^{n=N} \sum_{i=1}^{i=I} D_{jni}^k x_{ni}^k \quad \forall \quad j \tag{6b}$$

$$x_{ni}^k = \psi t_{ni}^k \tag{6c}$$

$$t_{ni}^k = \frac{1}{2}(l_{kni}^{out} - r_{kni}^{out} + l_{kn(i+1)}^{in} - r_{kn(i+1)}^{in}) \quad \forall \quad k, n, i \tag{6d}$$

$$0 \le r_{kni}^{in} \le r_{kni}^{out} \le \frac{t^{max}}{|K|}, \ 0 \le l_{kni}^{in} \le l_{kni}^{in} \le \frac{t^{max}}{|K|} \tag{6e}$$

$$r_{kni}^{out} + \Delta t \le r_{kn(i+1)}^{in}, \ l_{kni}^{out} + \Delta t \le l_{kn(i+1)}^{in} \tag{6f}$$

$$r_{kni}^{in} \le l_{kni}^{in}, \ r_{kni}^{out} \le l_{kni}^{out} \tag{6g}$$

–

- where $d_j$ is the dose in voxel j.
- where $\mathbf{x}$ is the set of beamlet intensities whose values are strictly positive i.e $\mathbf{x} \ge \mathbf{0}$ .
- K denotes the set of control points/beams orientations that are employed for irradiation during VMAT treatment. They correspond to the optimal beam orientations obtained from beam selection in section II-B.
- $|K|$ denoted the number of elements in K i.e. its cardinality
- $n \in N$ and $i \in I$ are the row and column indices respectively in the intensity matrix of an exposed beamlet at control point $k \in K$.
- $n$ also corresponds to the row index of MLC leaf pair.
- $D_{jni}^k$ is an element in the dose influence matrix $\mathbf{D}$. It denotes dose contribution to voxel $j$ from unit intensity of beamlet $(n, i)$ at the control point $k$. Each control point $k$ corresponds to a column in matrix $\mathbf{D}$ and each beamlet $(n, i)$ corresponds to a row in this matrix.
- $\psi$ is the machine dose rate in MUs$^{-1}$.
- $t_{ni}^k$ is the exposure time for beamlet $(n, i)$ in secs at beam $k$, $t^{max}$ is maximum delivery time.
- $t_{max}^k$ is the maximum allowed exposure time for all beamlets in beam $k$
- $r_{kni}^{in}$ and $l_{kni}^{in}$ denote the time at which the right and left leaf on row $n$ to arrive beamlet $(n, i)$ respectively
- $r_{kni}^{out}$ and $l_{kni}^{out}$ denote the time at which the right and left leaf on row $n$ to depart beamlet $(n, i)$ respectively.

The MLC leaf arrival and leaf departure time at each beamlet, which define the leaf trajectory, are the variables being optimized under this formulation. The model also takes into account the leaf constraints such as maximum MLC leaf speed, minimum MLC leaf motion per degree. The direct-leaf trajectory method for VMAT optimization avoids the two-step approach to VMAT seen in literature [8] [18] that can compromise treatment plan quality when

fluence intensities are converted to leaf positions during arc-sequencing. The optimization problem is approximately convex under this formulation, leading to solutions that can be obtained from available convex optimization solvers.

Below we will explain the constraints 6c -6g. Equation 6c defines the beamlet intensity as a product of the dose rate of the machine and the beamlet exposure time. Equation 6d is used to calculate the beamlet exposure time for all exposed beamlet from the arrival and departure times of the left and right MLC leaf. Equation 6e is a constraint for the ordering of the leaf arrival and departure times so that, for the left and right leaves in a row index, the departure time from a beamlet is always greater than the arrival time and positively bounded to a maximum exposure time period $t_{max}^k$. Equation 6f is a constraint on the maximum leaf speed moving from one beamlet to the next. Equation 6g keeps the arrival and departure times of the right MLC leaf behind the arrival and departure time of the leading left leaf.

*1) Gradient of the objective function:* We provide an expression for the gradient of our objective function in matrix notation by expanding equations 6b - 6d. We define a beamlet exposure vector $\mathbf{v}$ which is the variable of optimization and contains the leaf arrival and departure time for each beamlet. We also define an aperture matrix $\mathbf{M}$ that performs the linear mapping between the fluence intensity space $\mathbf{t}$ and the beamlet exposure space $\mathbf{v}$. Thus enabling equation 6d to be rewritten in matrix notation into equation 8.

$$\mathbf{v} = \begin{bmatrix} \mathbf{l}_{nb \times 1}^{out} \\ \mathbf{r}_{nb \times 1}^{out} \\ \mathbf{l}_{nb \times 1}^{in} \\ \mathbf{r}_{nb \times 1}^{in} \end{bmatrix}, \mathbf{M} = \begin{bmatrix} \mathbf{I}_{nb \times nb} & -\mathbf{I}_{nb \times nb} & \mathbf{S}_{nb \times nb} & -\mathbf{S}_{nb \times nb} \end{bmatrix} \tag{7}$$

$$\mathbf{t} = \mathbf{M}\mathbf{v} \tag{8}$$

$$\delta_{i,j} = \begin{cases} 1, & \text{if } i = j \\ 0, & \text{if } elsewhere \end{cases} \tag{9}$$

$$\mathbf{I}_{i,j} = \delta_{i,j} \tag{10}$$

$$\mathbf{S}_{i,j} = \delta_{i+1,j} \tag{11}$$

If we define $\delta_{ij}$ as the Kronecker delta function as equation 9, we can find expressions for $\mathbf{I}$ which is the identity matrix as in equation 10 and $\mathbf{S}$ which is the upper shift of the identity matrix as in equation 11. So the beamlet intensity defined in equation 6c can be rewritten in matrix notation:

$$\mathbf{x} = \delta \mathbf{t} \tag{12}$$

The matrix notation enables us to write the gradient of the objective function as:

$$\nabla f(\mathbf{d}) = \mathbf{D}^T (\frac{2p^+}{N_t}(\mathbf{d} - \mathbf{d}^p) + \frac{2p^-}{N_o}(\mathbf{d} - \mathbf{d}^p)) \tag{13}$$

*2) Jacobian of the constraints:* Similar to the objective function and its gradient, the constraints can be rewritten in matrix notation. This enables the manipulation of the algebraic expressions in matrix form that can be passed to the convex optimization solver. For example, constraint 6e can be re-written to a seperate bound constraint as in equation 15 and an inequality constraint as in equation 14.

$$l_{knj}^{in} - l_{knj}^{out} \leq \mathbf{0} \qquad (14)$$

$$\mathbf{0} \leq \mathbf{v} \leq \frac{t^{max}}{|K|} \qquad (15)$$

Equation 14 constraint can then be written in a matrix form as:

$$\mathbf{C1} = \begin{bmatrix} -\mathbf{I}_{nb \times nb} & \cdots & -\mathbf{0}_{nb \times nb} & \cdots & \mathbf{I}_{nb \times nb} & \cdots & -\mathbf{0}_{nb \times nb} \end{bmatrix} \tag{16}$$

Similar manipulations can be performed on the constraint equations 6e - 6g and the resulting matrices stacked to obtain the full constraint matrix $\mathbf{C}$ written as:

$$\mathbf{C} = \begin{bmatrix} -\mathbf{I}_{nb \times nb} & \cdots & -\mathbf{0}_{nb \times nb} & \cdots & \mathbf{I}_{nb \times nb} & \cdots & -\mathbf{0}_{nb \times nb} \\ \mathbf{0}_{nb \times nb} & \cdots & -\mathbf{I}_{nb \times nb} & \cdots & \mathbf{0}_{nb \times nb} & \cdots & \mathbf{I}_{nb \times nb} \\ \mathbf{I}_{nb \times nb} & \cdots & \mathbf{0}_{nb \times nb} & \cdots & -\mathbf{S}_{nb \times nb} & \cdots & \mathbf{0}_{nb \times nb} \\ \mathbf{0}_{nb \times nb} & \cdots & \mathbf{I}_{nb \times nb} & \cdots & \mathbf{0}_{nb \times nb} & \cdots & -\mathbf{S}_{nb \times nb} \\ \mathbf{0}_{nb \times nb} & \cdots & \mathbf{0}_{nb \times nb} & \cdots & -\mathbf{I}_{nb \times nb} & \cdots & \mathbf{I}_{nb \times nb} \\ -\mathbf{I}_{nb \times nb} & \cdots & \mathbf{I}_{nb \times nb} & \cdots & \mathbf{0}_{nb \times nb} & \cdots & \mathbf{0}_{nb \times nb} \end{bmatrix} \tag{17}$$

These constraints are verified by a linearly projecting intermediate solutions of the beamlet exposure vector $\mathbf{v}$ on the constraint matrix $\mathbf{C}$ using:

$$g(\mathbf{v}) = \mathbf{Cv} \tag{18}$$

Therefore the constraint jacobian which we pass to the convex optimizer can be written as:

$$\frac{\partial g}{\partial \mathbf{v}} = \mathbf{C} \tag{19}$$

*3) Definition of Upper bound for exposure time:* Direct leaf trajectory optimization requires an upper bound for the exposure time $t_{max}^k$ as seen in constraint 6e at each control point $k$. For our implementation, we define the maximum exposure time as the time it takes the trailing multileaf collimator leaf to leave the furtherest exposed beamlet. This is obtained using the limit position of the left and right leaf of each row of the multileaf collimator in the beam-eye-view (BEV) aperture to determine the maximum time leaf traversal time in each row. The relationship is obtained using:

$$\mathbf{t}_{row\_max}^k = \frac{\mathbf{l}_{max} - \mathbf{r}_{max}}{s_{leaf}} \tag{20}$$

where $\mathbf{t}_{row\_max}^k$ is a vector of the maximum allowed traversal time of each row of multileaf collimator leaf pairs that have their beamlets exposed, $\mathbf{l}_{max}$ and $\mathbf{r}_{max}$ are the limit positions (mm) of the left and right leaves in the BEV aperture and $s_{leaf}$ is the leaf speed.

The upper bound for the exposure time is calculated by a summation of the time taken by the slowest multileaf collimator pair at a control point and the time taken to move from one control point to the next.

$$t_{max}^k = \max(\mathbf{t}_{row\_max}^k) + \frac{\Delta\Theta_{k,k+1}}{g_s} \tag{21}$$

where $\Delta\Theta_{k,k+1}$ is the angular distance from one control point to the next and $g_s$ is the angular speed of the gantry. For this work, it is assumed that the couch moves at the same speed as the gantry for all VMAT optimizations performed.

*4) Estimating the delivery time:* The delivery time is estimated as the sum of the delivery time for each control point (maximum MLC row exposure time) and the time taken for the gantry to move from one control point to the next. This is closely related to equation 20 and is given by the equation:

$$t = \sum_{k=1}^{k=K} \max(\mathbf{t}_n^k) + \frac{\Delta\Theta_{k,k+1}}{g_s} \tag{22}$$

where $\mathbf{t}_n^k$ is a vector of the traversal time of each row $n$ of the multileaf collimator leaf pair that has its beamlets exposed in a control point during treatment. $\mathbf{t}_n^k$ is calculated from the beamlet exposure vector resulting from the direct leaf trajectory optimizer by summing the exposure time of all beamlets in each row.

$$\mathbf{t}_n^k = \sum_{i=1}^{i=I} t_{ni}^k \tag{23}$$

### D. Implementation

Our computations were performed on a computer with Intel® Xeon® 16-core W-2145 3.7GHz processor and 256GB random access memory (RAM). The non-coplanar VMAT treatment planning experiments were performed using matRad [19] a toolkit for radiotherapy computational research and the research code was written in Matlab (version 2017a). The VMAT optimization is solved using an ipopt [20] implementation of L-BFGS algorithmn [21] that is included in matRad. For comparison purpose the standard non-coplanar VMAT planning method proposed in [9] was implemented in matRad. The main difference with the proposed method is that the beam selection is achieved using a greedy approach.

### E. Evaluation study

*1) Parameters:* We assume that the couch and gantry move at the same speed during the treatment. The beamlet size is set to $7 \times 7 \ mm^2$ and MLC size of $40 \times 40 \ cm$ is used. This beamlet size was chosen so as to reduce the size of the dose influence matrix due to main memory limitations of the computer. The MLC size chosen is the standard size available from most equipment manufacturers to enable comparison. Machine parameters used for the direct leaf trajectory optimization was for a 6MV Linac delivering photon beams. The Linac is set to 600 $MU/min$ for the max dose rate, 3 $cm/sec$ for the max leaf speed and 6 $deg/sec$ for the max gantry and couch speed. We also set the LINAC collimator angle to $0°$.

*2) Data sets:* Three data sets, one from the American Association of Physicists in Medicine Task Group 119 (AAPM TG-119) benchmark [22] and two from clinical cases in prostate and liver cancers were considered as benchmark for treatment plan evaluation using our proposed beam selection method. The AAPM TG-119 benchmark is particularly adapted for studying and comparing non-coplanar treatment planning using a C-shaped target surrounding by an area of OAR. Patients CT data and the associated labeled segmentation for the prostate and liver cancer cases were obtained from the CORT dataset [23]. The prescribed dose and the candidate beam orientations, defined as couch-gantry angle pairs, are also provided from the CORT dataset. The candidate beam orientations consist of 1983 non-coplanar beam angles sampled at $5°$ discretization. The dose influence matrix for each evaluation cases was calculated using the pencil-beam algorithm implemented in matRad. The dose calculation of all 1983 candidate beams in matRad differs depending on the case under consideration and the matrix size of the CT, the speed and memory of the computer. e.g for the prostate case of size 187x187x90, we utilized 50GB RAM on a PC equipped with 256GB RAM and a computation time of 59.3 minutes. All cases have a target prescription dose of 50Gy. Within the cost function, the dose to the OAR is set to 0Gy, in order to have the lowest dose after optimisation within the OAR. The importance factor are chosen by trial-and-error as $p^+ = 1000$ for the tumor voxels and $p^- = 10$ for the organ-at-risk voxels except for the skin voxels which is set as $p^- = 400$ in order to select beams that are not too close to each other.

*3) Evaluations:* For comparison, treatment plans for the three benchmark cases was also made using the non-coplanar VMAT method [9] that uses a greedy beam selection strategy and a coplanar VMAT method with a fixed couch orientation. The greedy algorithm has no restriction on the number of iterations, or the number of beams angles required. The greedy algorithm is stopped only when a $5\%$ increase in the final objective function value is detected in comparison to the most recent final objective function value. To keep comparison similar, the same objective function, importance factors and parameters are employed for all treatment plans.

The coplanar VMAT beam trajectory consists of a single arc containing 37 beam angles that are obtained from the space of the candidate beam orientations used in the CORT dataset described in sub-section II-E2. This is done to keep the comparison to the non-coplanar beam trajectory similar by maintaining the same angular distance as the coplanar trajectory. The gantry angles for the coplanar plan ranges between $(-90° \leq 0° \leq 90°)$ and are selected from the space of candidate beam orientations where the couch angles is $0°$.

Results from the proposed SA method, non-coplanar greedy approach and the coplanar method were compared using several criteria. The mean of the dose and the maximum of the dose absorbed by all voxels in each labeled organ were calculated based on the dose map recovered from each the optimized plans. Dose Volume Histogram (DVH) for each of these organs between the three methods were also compared. In order to quantitatively assess the degree of conformity of delivered dose, the conformity number proposed by [24] was

used. It is given as:

$$CN = \frac{V_{T,ref}}{V_T} \times \frac{V_{T,ref}}{V_{ref}} \qquad (24)$$

where $V_{ref}$ is the volume that receives a dose equal to or greater than the reference dose, $V_{T,ref}$ is the volume of target that receives a dose equal to or greater than the reference dose and $V_T$ is the volume of the target. The conformity number ranges from 0 to 1. A value of 1 denotes that an exact prescription dose has been delivered to the target with no dose to the surrounding tissues while 0 denotes a non-conformal dose distribution. Finally, the theoretical delivery time for each optimized plan was estimated using the relationships defined in section II-C4.

## III. RESULTS

Dosemap obtained after beam optimization for the different cases and for the different methods are in figures 1. Comparison of the Dose Volume Histogram (DVH) for the coplanar method and non-coplanar SA method are in figure 3. Statistical data on the different planning (delivery time, conformity number, etc.) for every case are in table I, when the dose values are listed in table II.

### A. TG119 case study

A better conformal dose is observed from the PTV dose contours when using the SA method. Inside the C-shape, a lower dose is also observed. This is confirmed by the conformity number of 0.88 and 0.91 for the co-planar and the greedy non-coplanar method respectively and 0.92 for the non-coplanar SA method. Similarly, there is a reduction in the mean dose within the core confirmed by the DVH, where the mean dose in the core was 18.9Gy, 12.3Gy and 4.7Gy for the coplanar and non-coplanar greedy method and non-coplanar SA methods respectively. Coplanar optimisation leads to a higher mean dose in the core compared to the non-coplanar greedy method up to 35%. However, non-coplanar SA method performed a better reduction compared to the coplanar method up to 52% within the core. Considering the estimated delivery time the treatment planned with a beam selection done by non-coplanar SA method was longer with 227s than coplanar method with 183s and non-coplanar greedy method with 140s. This is explained by the higher number of control points 92 for non-coplanar SA method, 26 for non-coplanar greedy method and 37 for coplanar method. Larger angular distances between control points selected using the SA method also contribute to an increase in the estimated delivery time.

### B. Liver case study

Same conclusion to the liver case can be drawn. Dosemaps show a conformal dose improvement in favor to non-coplanar SA method. Since there are larger number of control point with the non-coplanar SA method, there are less hot spots around the PTV and a longer beam trajectory. A conformity number of 0.93 and 0.9 was found for the coplanar and non-coplanar Greedy method respectively when a value of 0.95
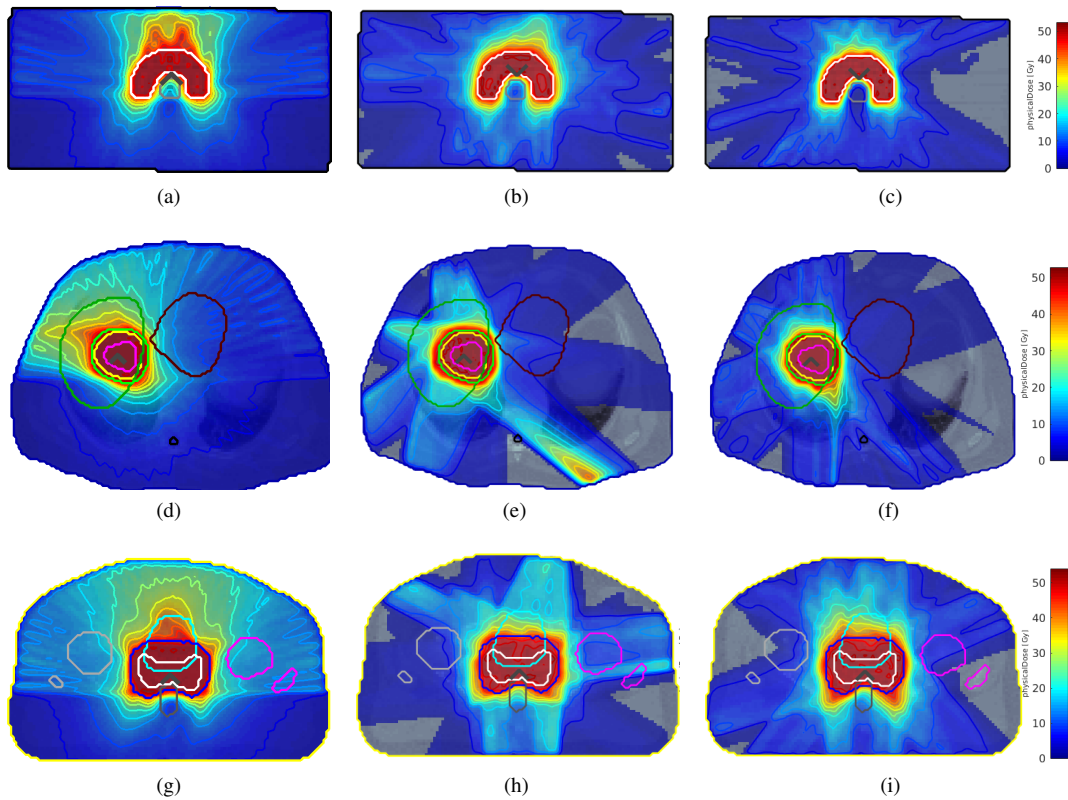
Figure 1: Comparing Axial isodose contours for TG119 case (first row), liver case (second row) and prostate case (third row) using coplanar method (first column), non-coplanar greedy method (second column) and non-coplanar SA method (third column).

Table I: Statistics on resulted planning after optimization for the three case studies

| Metric | TG119 | | | Liver case | | | Prostate case | | |
|---|---|---|---|---|---|---|---|---|---|
| | Coplanar | Non-coplanar | | Coplanar | Non-coplanar | | Coplanar | Non-coplanar | |
| | | Greedy | SA | | Greedy | SA | | Greedy | SA |
| Estimated Delivery time | 183s | 140s | 227s | 145s | 127s | 132s | 246s | 87s | 127s |
| Nb. of Control Point | 37 | 26 | 92 | 37 | 43 | 31 | 37 | 10 | 43 |
| Obj. function value | $2.55\times10^4$ | $1.71\times10^4$ | $1.64\times10^4$ | $9.63\times10^3$ | $1.05\times10^4$ | $9.54\times10^3$ | $4.72\times10^4$ | $7.24\times10^4$ | $6.88\times10^4$ |
| Conformity number | 0.88 | 0.91 | 0.92 | 0.93 | 0.9 | 0.95 | 0.55 | 0.5 | 0.49 |

was obtained for the SA method. As shown on DVH and dose values, most of the organs-at-risk (OAR) received less dose with the beam selection with SA method than the one with Greedy method. This dose reduction reached 12% for the skin, 38% for the heart, and 60% for the duodenum. The most improvement was for the spinal cord, where the dose was reduced by 80% when SA method is used instead of the greedy method. However, this gain was at the cost of an increase in the estimated delivery time that reached 132s with SA method vs 127s for the Greedy method. Again, this was explained by the fact that a higher number of control points which are farther apart from each other was selected with SA method. In this case coplanar method provided better dose reduction in the celiac, duodenum and SMASV. However, due to the higher number of control points, the delivery time of the coplanar method was longer to the non-coplanar SA method.

## C. Prostate case study

Similarly to the previous cases, the same conclusion was observed with the prostate case. Although, SA method clearly improved dose conformation, especially for the beam entry point around the PTV, the conformity number was lower than the Greedy method: 0.49 for SA method and 0.5 for Greedy method. The dose value to the PTV was the same with both the coplanar and non-coplanar greedy method, 49.4Gy. However, non-coplanar SA method provided a treatment plan with lower dose on the OAR. Doses were reduced by 4% in the bladder, 13% in the rectum and 21.0% and penile bulb compare to the dose recovered with the Greedy method. Non-coplanar SA was not able to reduce the dose within the penile bulb compared to the coplanar method. This was probably because of the better avoidance of the femoral heads by the non-coplanar SA method, with a decrease of the dose of 71.6% and 73.0% for the left and right femoral heads respectively compare to the coplanar method. For clinical application penalty factor should
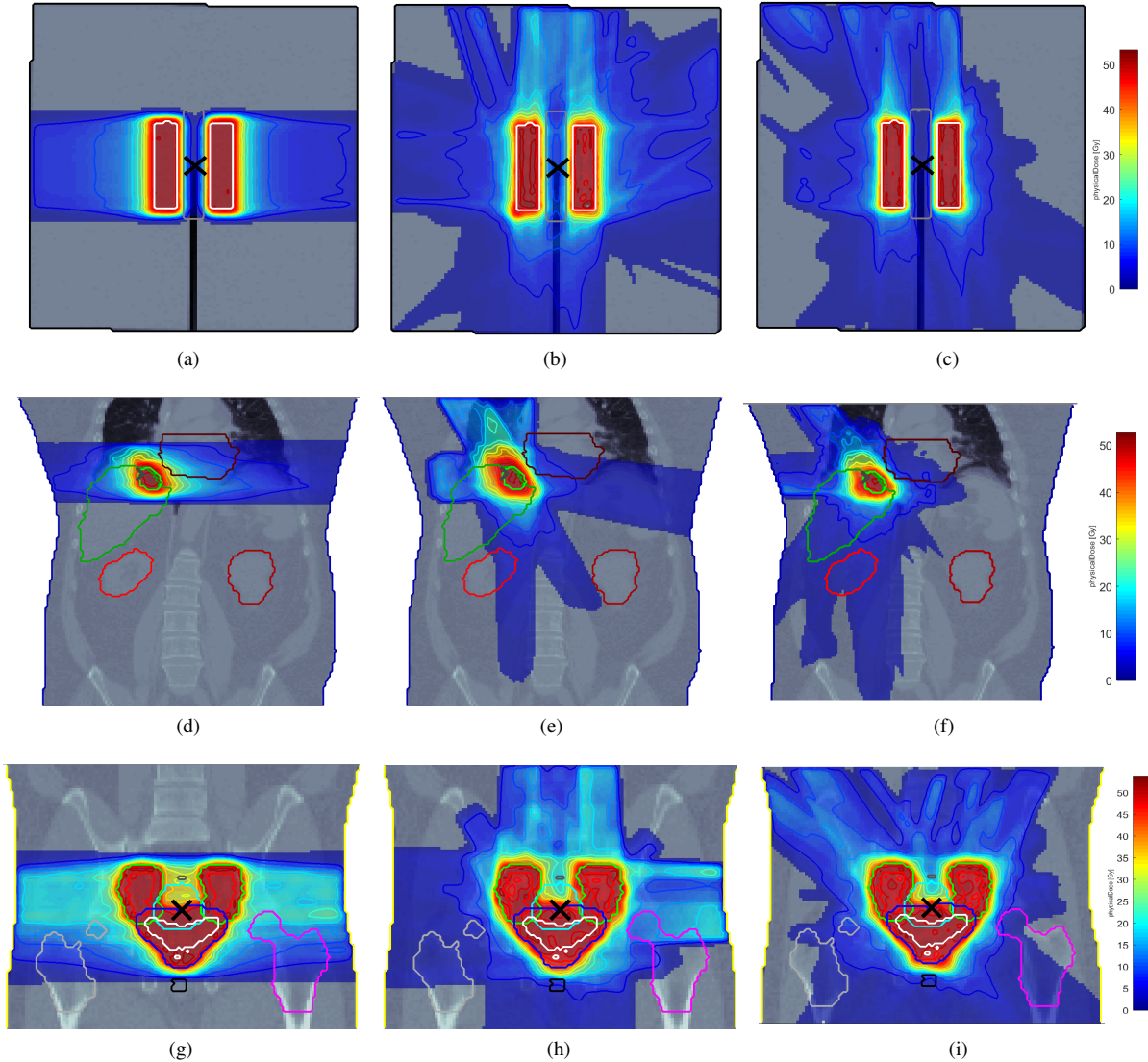
Figure 2: Comparing Coronal isodose contours for TG119 case (first row), liver case (second row) and prostate case (third row) using coplanar method (first column), non-coplanar greedy method (second column) and non-coplanar SA method (third column).

be introduced to take care of which organ to spare in priority. Coplanar method was the longer to deliver with 246s, compare to 127s for the non-coplanar SA method and only 87s for the non-coplanar greedy method.

## IV. DISCUSSION AND CONCLUSION

The use of beam angle selection to generate non-coplanar trajectories for VMAT presents an opportunity to search a larger space to obtain optimal beam orientations for treatment. The consequence is that a huge number of solutions are possible to the resulting non-convex combinatorial optimization problem. The simulated annealing algorithm for non-coplanar VMAT treatment planning that we have presented is able to handle the problem of non-convexity by employing direct leaf trajectory optimization. The proposed algorithm has no restriction on the search space and thereby evaluates a very large number of possible treatment plans. This allows the

optimizer to escape local minima in order to give a solution that is "closer" to the globally optimal treatment plan.

Dosimetric improvements in terms of organ at risk sparing was observed using the SA method compared to the standard greedy method, such as: reduced mean dose to the core in TG-119 case by 62%, the heart and the spinal cord in liver case by 38% and 80% respectively, the rectum and the penile bulb in prostate case by 13% and 21% respectively. However, no significant differences are observed in the dose delivered to the target in all cases ($49.6 Gy$).

For these particular benchmark cases the SA method showed better organ-at-risk sparing compared to the coplanar method e.g reduced mean dose to the heart in the liver case, to the rectum, bladder and femoral heads in prostate case and to the core in the TG-119 case. However, this was not the case for some organs-at-risk, such as the celiac and the duodenum in the liver case and the skin and the penile bulb in the prostate
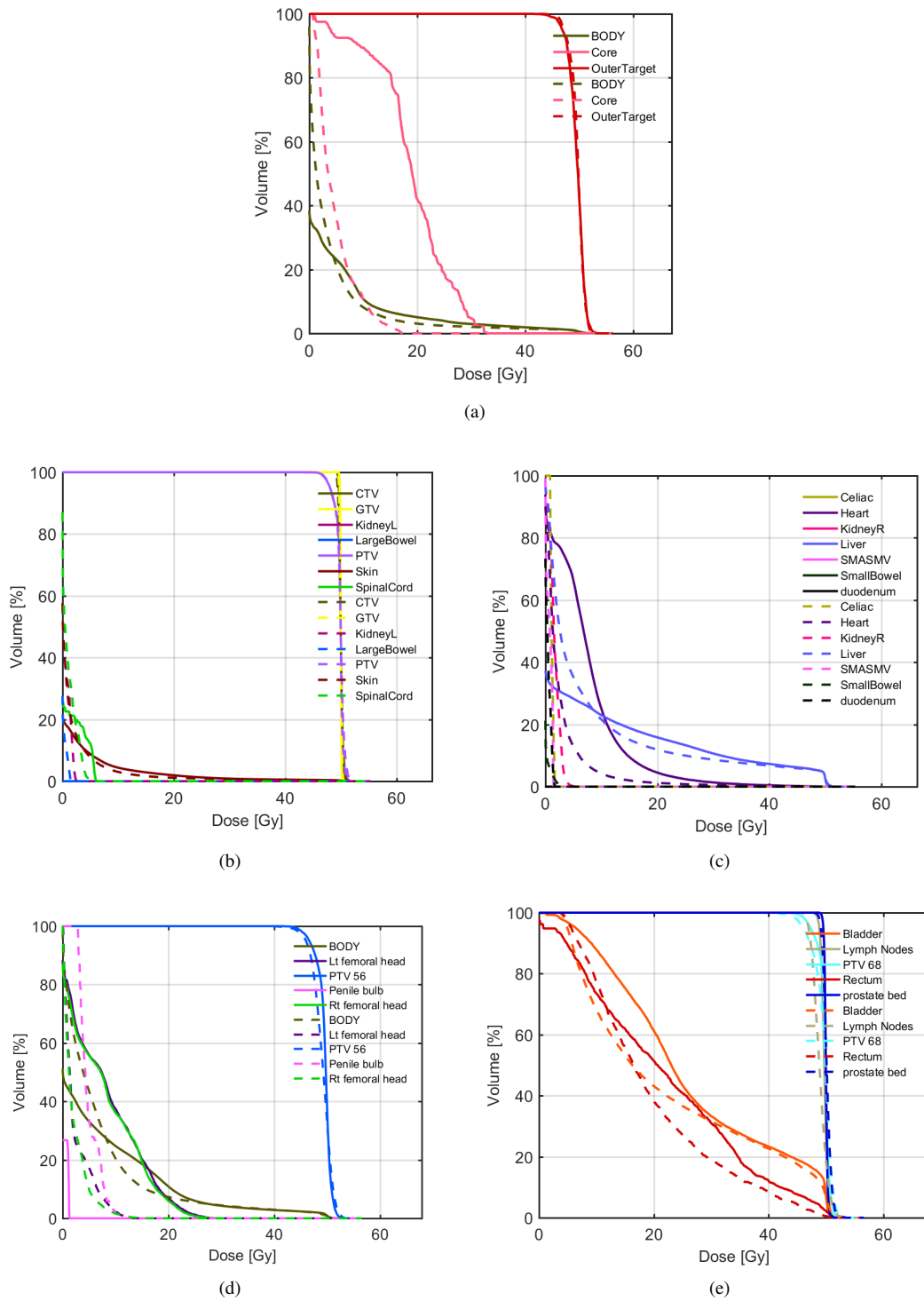
Figure 3: DVH comparing the coplanar method (thick lines) to non-coplanar SA method (dashed lines) for the TG119 case (first row), the liver case (second row) and the prostate case (third row).

case. This difference in organ-at-risk sparing is reflected in the conformity number. An explanation is that these solutions from the coplanar method are locally optimal and is a function of the trajectory chosen for these experiments. The SA method in the search for global optimality may counter balance the sparing of one organs-at-risk with a higher mean dose to another organ-at-risk.

Although interesting results were obtained, a further clinical investigation is needed to confirm the improvement brings by the SA method and non-coplanar treatment. Our next step will be to perform a complete dosimetric comparison using a large number of patients targeting different tumors localization, such prostate, liver and brain.

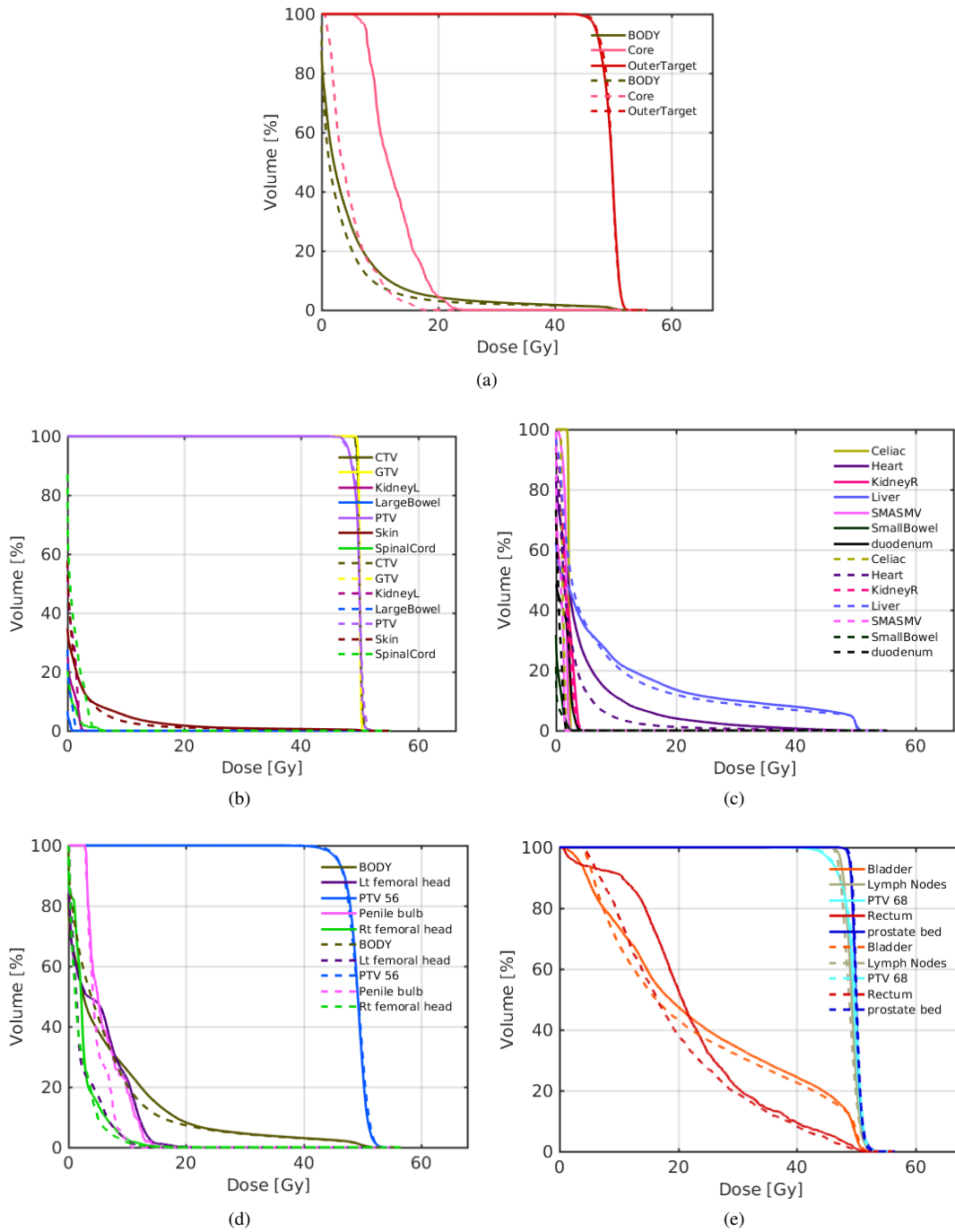We found that there is an increase in the number of control

Figure 4: DVH comparing the greedy method (thick lines) to non-coplanar SA method (dashed lines) for the TG119 case (first row), the liver case (second row) and the prostate case (third row).

points when using the proposed non-coplanar SA method compared to the Greedy method. Although the estimated delivery time was increased with the non-coplanar SA method, between 24% to 46% longer than standard non-coplanar VMAT, this is not a limitation to be deployed in clinical routine, especially if we consider the benefits of the dose sparing to OAR. In addition, the delivery time of the non-coplanar SA method was faster than the coplanar method, of 9% for the liver case and 48% for the prostate case.

This is interesting because non-coplanar method does not

always mean longer delivery time. And, on the other hand, non-coplanar method does not always mean better organs-at-risk sparing. This was the case for the liver and prostate cases, where the coplanar method performed better dose reduction for some organs. This demonstrates that depending on the patient case, our proposed non-coplanar VMAT optimization method can be more clinically interesting that coplanar method.

Table II: Dose values for each organs after optimization for the three case studies. Bold values are the best mean dose values obtained for each organs by comparing the three different optimization methods.

| Case study | Target | Coplanar method Dose [Gy] | | Non-coplanar Greedy method Dose [Gy] | | Non-coplanar SA method Dose [Gy] | |
|---|---|---|---|---|---|---|---|
| | | Mean | Max | Mean | Max | Mean | Max |
| TG119 | | | | | | | |
| | PTV | 49.5 | 53.5 | 49.5 | 52.8 | **49.6** | 52.3 |
| | Core | 18.9 | 32.9 | 12.3 | 24.2 | **4.7** | 17.6 |
| | Body | **3.7** | 53.5 | 4.8 | 52.8 | **3.7** | 52.3 |
| Liver | | | | | | | |
| | PTV | 49.7 | 51.8 | 49.7 | 51.9 | **49.9** | 51.4 |
| | Celiac | **≈0.0** | ≈0.0 | 2.1 | 2.4 | 1.1 | 1.6 |
| | Heart | 7.5 | 50.6 | 4.2 | 50 | **2.6** | 51 |
| | Spinal cord | 1.0 | 5.0 | 1.0 | 6.2 | **0.2** | 5.0 |
| | Duodenum | **≈0.0** | ≈0.0 | 1.0 | 4.8 | 0.4 | 1.8 |
| | SMASV | **≈0.0** | ≈0.0 | 1.6 | 2.4 | 0.7 | 1.4 |
| | Skin | **1.5** | 51.8 | 1.7 | 51.9 | **1.5** | 52.6 |
| Prostate | | | | | | | |
| | PTV | **49.4** | 53.1 | **49.4** | 56.2 | 49 | 53.1 |
| | Skin | **6.4** | 53.1 | 6.9 | 53.8 | 6.9 | 53.8 |
| | Bladder | 26.2 | 52.3 | 23.5 | 53.5 | **22.5** | 53.7 |
| | Rectum | 21.8 | 51.6 | 22.4 | 50.9 | **19.5** | 51.6 |
| | Penile bulb | **0.3** | 1.2 | 6.2 | 14.5 | 4.9 | 10.6 |
| | Left femoral head | 8.1 | 30.8 | 5.0 | 22.4 | **2.3** | 14.6 |
| | Right femoral head | 7.8 | 31.3 | 2.6 | 20.1 | **2.1** | 17.3 |

≈ 0: values are too small to be significant, and were considered close to 0.

REFERENCES

[1] K. Otto, "Volumetric modulated arc therapy: IMRT in a single gantry arc," *Medical physics*, vol. 35, no. 1, pp. 310–317, 2008.
[2] K. Sheng, D. M. Shepard, and C. G. Orton, "Noncoplanar beams improve dosimetry quality for extracranial intensity modulated radiotherapy and should be used more extensively," *Medical physics*, vol. 42, no. 2, pp. 531–533, 2015.
[3] C. Audet, B. A. Poffenbarger, P. Chang, P. S. Jackson, R. E. Lundahl, S. I. Ryu, and G. R. Ray, "Evaluation of volumetric modulated arc therapy for cranial radiosurgery using multiple noncoplanar arcs," *Medical physics*, vol. 38, no. 11, pp. 5863–5872, 2011.
[4] E. Orlandi, T. Giandini, E. Iannacone, E. De Ponti, M. Carrara, V. Mongioj, C. Stucchi, S. Tana, P. Bossi, L. Licitra *et al.*, "Radiotherapy for unresectable sinonasal cancers: dosimetric comparison of intensity modulated radiation therapy with coplanar and non-coplanar volumetric modulated arc therapy," *Radiotherapy and Oncology*, vol. 113, no. 2, pp. 260–266, 2014.
[5] K. Woods, D. Nguyen, A. Tran, Y. Y. Victoria, M. Cao, T. Niu, P. Lee, and K. Sheng, "Viability of noncoplanar vmat for liver sbrt compared with coplanar vmat and beam orientation optimized 4π imrt," *Advances in radiation oncology*, vol. 1, no. 1, pp. 67–75, 2016.
[6] G. Smyth, P. M. Evans, J. C. Bamber, and J. L. Bedford, "Recent developments in non-coplanar radiotherapy," *The British journal of radiology*, vol. 92, no. 1097, p. 20180908, 2019.
[7] J. Unkelbach, T. Bortfeld, D. Craft, M. Alber, M. Bangert, R. Bokrantz, D. Chen, R. Li, L. Xing, C. Men *et al.*, "Optimization approaches to volumetric modulated arc therapy planning," *Medical physics*, vol. 42, no. 3, pp. 1367–1377, 2015.
[8] E. Wild, M. Bangert, S. Nill, and U. Oelfke, "Noncoplanar VMAT for nasopharyngeal tumors: Plan quality versus treatment time," *Medical physics*, vol. 42, no. 5, pp. 2157–2168, 2015.
[9] D. Papp, T. Bortfeld, and J. Unkelbach, "A modular approach to intensity-modulated arc therapy optimization with noncoplanar trajectories," *Physics in medicine and biology*, vol. 60, no. 13, p. 5179, 2015.

[10] M. Langhans, J. Unkelbach, T. Bortfeld, and D. Craft, "Optimizing highly noncoplanar vmat trajectories: the novo method," *Physics in Medicine & Biology*, vol. 63, no. 2, p. 025023, 2018.
[11] Q. Lyu, Y. Y. Victoria, D. Ruan, R. Neph, D. O'Connor, and K. Sheng, "A novel optimization framework for vmat with dynamic gantry couch rotation," *Physics in Medicine & Biology*, vol. 63, no. 12, p. 125013, 2018.
[12] D. Papp and J. Unkelbach, "Direct leaf trajectory optimization for volumetric modulated arc therapy planning with sliding window delivery," *Medical physics*, vol. 41, no. 1, p. 011701, 2014.
[13] L. Ingber, "Simulated annealing: Practice versus theory," *Mathematical and computer modelling*, vol. 18, no. 11, pp. 29–57, 1993.
[14] M. Bangert, P. Ziegenhein, and U. Oelfke, "Characterizing the combinatorial beam angle selection problem," *Physics in medicine and biology*, vol. 57, no. 20, p. 6707, 2012.
[15] K. A. Mountris, J. Bert, and D. Visvikis, "Prostate brachytherapy optimization using gpu accelerated simulated annealing and monte carlo dose simulation," in *Nuclear Science Symposium, Medical Imaging Conference and Room-Temperature Semiconductor Detector Workshop (NSS/MIC/RTSD), 2016*. IEEE, 2016, pp. 1–2.
[16] D. Bertsimas, J. Tsitsiklis *et al.*, "Simulated annealing," *Statistical science*, vol. 8, no. 1, pp. 10–15, 1993.
[17] H. Sanvicente-Sánchez and J. Frausto-Solís, "A method to establish the cooling scheme in simulated annealing like algorithms," in *International Conference on Computational Science and Its Applications*. Springer, 2004, pp. 755–763.
[18] H. E. Romeijn, R. K. Ahuja, J. F. Dempsey, and A. Kumar, "A column generation approach to radiation therapy treatment planning using aperture modulation," *SIAM Journal on Optimization*, vol. 15, no. 3, pp. 838–862, 2005.
[19] E. Cisternas, A. Mairani, P. Ziegenhein, O. Jäkel, and M. Bangert, "matrad-a multi-modality open source 3d treatment planning toolkit," in *World Congress on Medical Physics and Biomedical Engineering, June 7-12, 2015, Toronto, Canada*. Springer, 2015, pp. 1608–1611.
[20] A. Wächter and L. T. Biegler, "On the implementation of an interior-point filter line-search algorithm for large-scale nonlinear programming," *Mathematical programming*, vol. 106, no. 1, pp. 25–57, 2006.
[21] C. Zhu, R. H. Byrd, P. Lu, and J. Nocedal, "Algorithm 778: L-bfgs-b: Fortran subroutines for large-scale bound-constrained optimization," *ACM Transactions on Mathematical Software (TOMS)*, vol. 23, no. 4, pp. 550–560, 1997.
[22] G. A. Ezzell, J. W. Burmeister, N. Dogan, T. J. LoSasso, J. G. Mechalakos, D. Mihailidis, A. Molineu, J. R. Palta, C. R. Ramsey, B. J.

Salter *et al.*, "Imrt commissioning: multiple institution planning and dosimetry comparisons, a report from aapm task group 119," *Medical physics*, vol. 36, no. 11, pp. 5359–5373, 2009.

[23] D. Craft, M. Bangert, T. Long, D. Papp, and J. Unkelbach, "Shared data for intensity modulated radiation therapy (IMRT) optimization research: The CORT dataset," *GigaScience*, vol. 3, p. 37, 2014.

[24] A. Van't Riet, A. C. Mak, M. A. Moerland, L. H. Elders, and W. Van Der Zee, "A conformation number to quantify the degree of conformality in brachytherapy and external beam irradiation: application to the prostate," *International Journal of Radiation Oncology\* Biology\* Physics*, vol. 37, no. 3, pp. 731–736, 1997.